NANO MICRO small

Supporting Information

for *Small,* DOI: 10.1002/smll.202203723

Biofunctional Nanodot Arrays in Living Cells Uncover Synergistic Co-Condensation of Wnt Signalodroplets

Michael Philippi, Christian P. Richter, Marie Kappen, Isabelle Watrinet, Yi Miao, Mercedes Runge, Lara Jorde, Sergej Korneev, Michael Holtmannspötter, Rainer Kurre, Joost C. M. Holthuis, K. Christopher Garcia, Andreas Plückthun, Martin Steinhart, Jacob Piehler,* and Changjiang You**

Supporting Information

Biofunctional nanodot arrays in living cells uncover synergistic co-condensation of Wnt signalodroplets

Michael Philippi,[1] Christian P. Richter[1], Marie Kappen[1], Isabelle Watrinet[1], Yi Miao[2], Mercedes Runge,[1] Lara Jorde[1], Sergej Korneev[1], Michael Holtmannspötter[1], Rainer Kurre[1], Joost C. M. Holthuis[1], K. Christopher Garcia[2], Andreas Plückthun[3], Martin Steinhart[1]*, Jacob Piehler[1]*, Changjiang You[1]*

[1] Department of Biology/Chemistry and Center of Cellular Nanoanalytics (CellNanOs), Osnabrück University, 49076 Osnabrück, Germany

[2] Department of Molecular and Cellular Physiology, Department of Structural Biology, Howard Hughes Medical Institute, Stanford University School of Medicine, Stanford, CA 94305, USA

[3] Department of Biochemistry, University of Zurich, Winterthurerstr. 190, 8057 Zurich, Switzerland

*Corresponding authors: cyou@uni-osnabrueck.de; piehler@uos.de; martin.steinhart@uos.de

SUPPLEMENTARY FIGURES

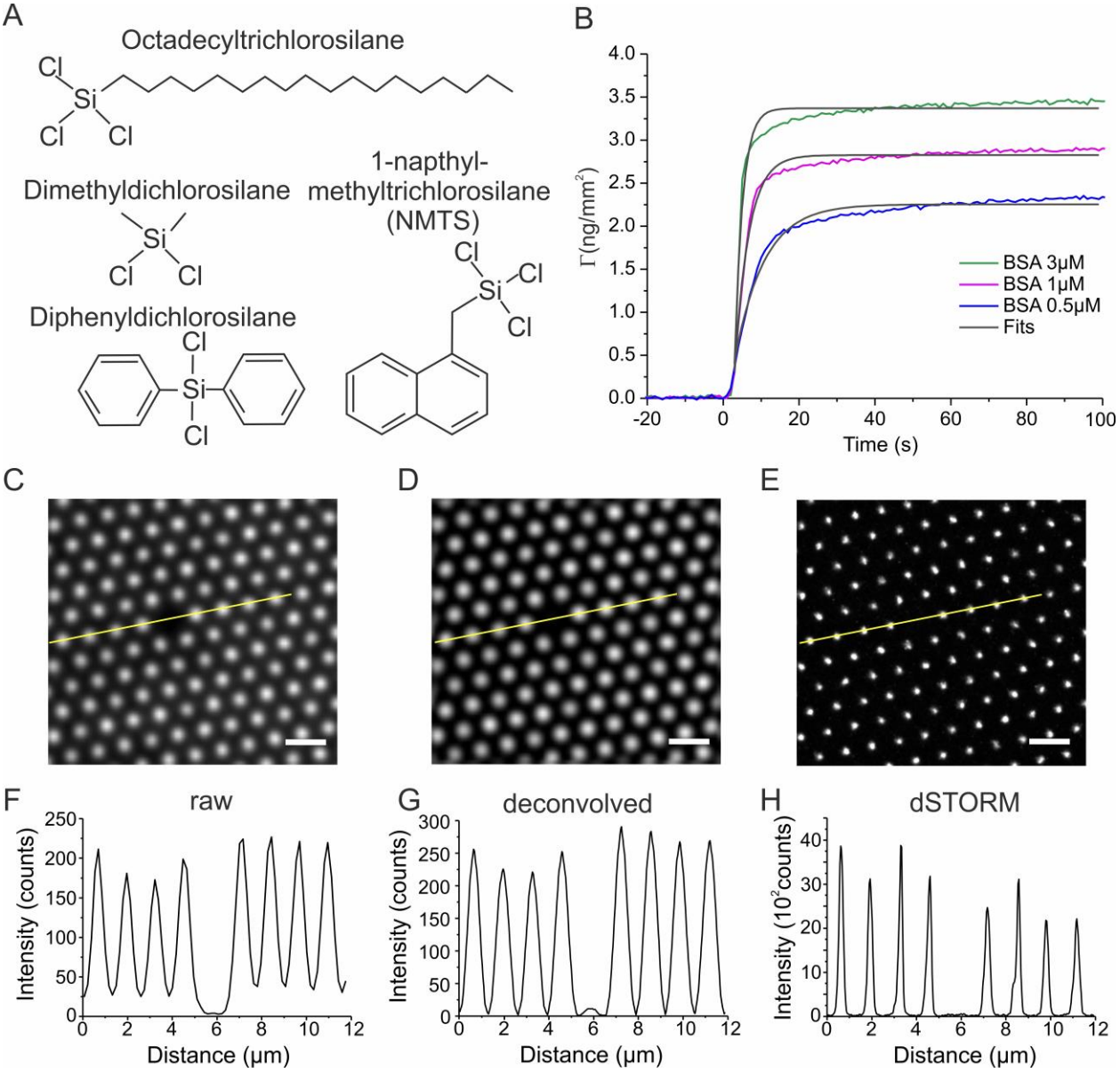

Fig. S1 Surface modification for high-contrast protein nanopatterning by capillary nanostamping. (A) Chemical structures of silanes used for rendering silica substrates hydrophobic. (B) Binding of BSA on NMTS-coated silica monitored in real-time by reflectance interference (RIF) detection under flow-through conditions. An association rate constant k_a = 2.7×10^5 $M^{-1}s^{-1}$ was estimated from the fit (Table S1). (C-H) Signal and contrast of representative nanodot arrays (NDAs) obtained by printing ^{AT647N}BSA assessed by fluorescence microscopy. Raw TIRF microscopy image (C), Deconvolved TIRF microscopy image (D) and dSTORM image (E). Scale bar 2 μm. Corresponding intensity profiles highlighted in the yellow line in the corresponding images for the raw (F), the deconvolved (G) and the dSTORM (H) images. The true background can be estimated in the defect region.

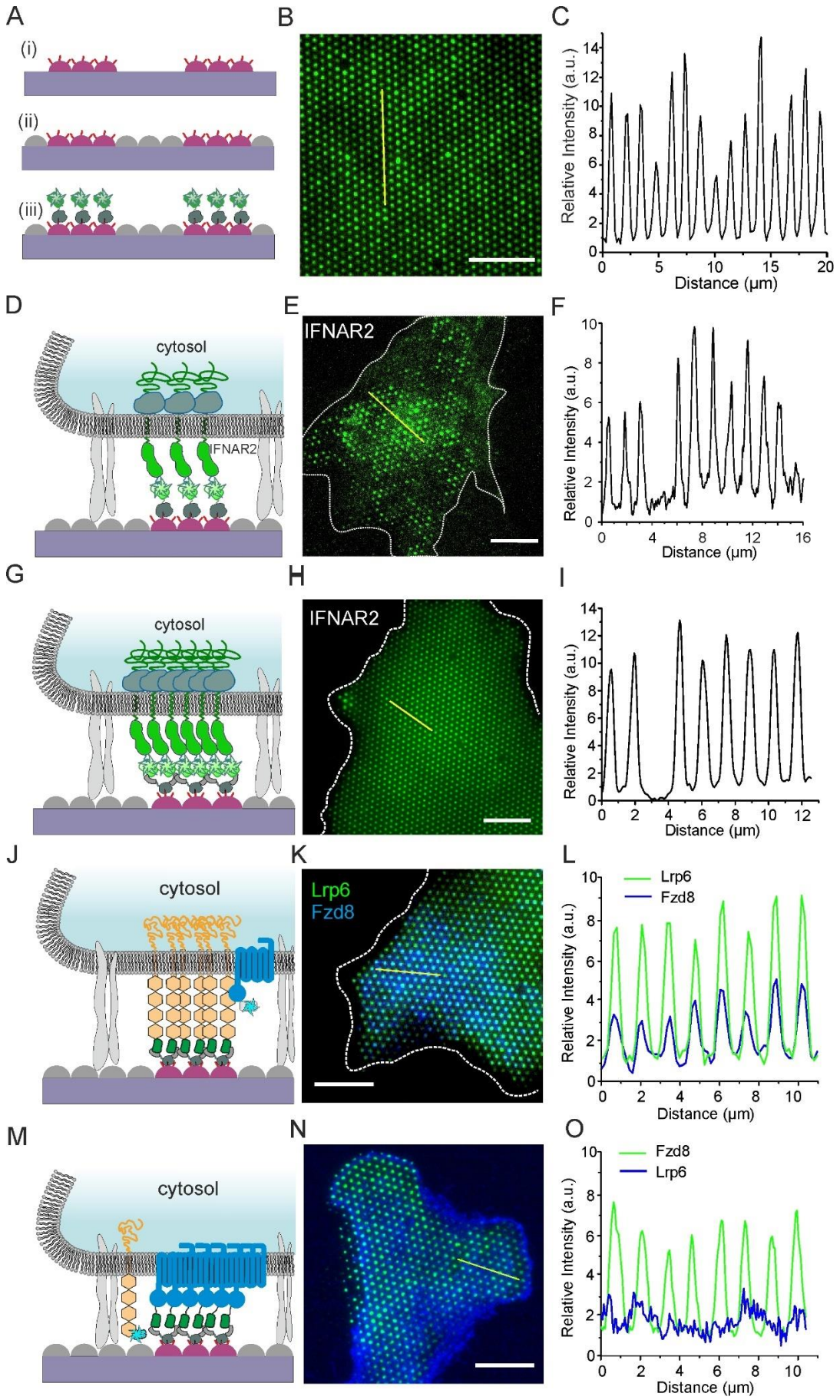
A
(i)
(ii)
(iii)
B
C
Relative Intensity (a.u.)
Distance (μm)
D
cytosol
IFNAR2
E
IFNAR2
F
Relative Intensity (a.u.)
Distance (μm)
G
cytosol
H
IFNAR2
I
Relative Intensity (a.u.)
Distance (μm)
J
cytosol
K
Lrp6
Fzd8
L
Lrp6
Fzd8
Relative Intensity (a.u.)
Distance (μm)
M
cytosol
N
O
Fzd8
Lrp6
Relative Intensity (a.u.)
Distance (μm)

Fig. S2 Capturing strategies into bNDAs via HaloTag and tdClamp *in vitro* and *in cellulo*. (A-C) Fluorescence staining of ^{HTL}BSA bNDAs by reaction with HaloTag-mEGFP. (A) Cartoon of the surface architecture with ^{HTL}BSA dots (red), FCS backfilling (grey) and HaloTag-mEGFP (green). (B) Representative TIRF microscopy image. Scale bar 10 µm. (C) Intensity profile along the yellow line highlighted in panel A. (D-F) Formation of Type-I interferon receptor bNDAs in live cells via ^{HTL}BSA functionalization. (D) Cartoon of capturing HaloTag-mEGFP-IFNAR2 on ^{HTL}BSA bNDAs. (E) TIRF microscopy image of HaloTag-mEGFP-IFNAR2 bNDAs in live cell. (F) Intensity profile along the yellow line highlighted in panel E. (G-I) Formation of Type-I interferon receptor bNDAs via tdClamp functionalization. (G) Cartoon of capturing HaloTag-mEGFP-IFNAR2 on tdClamp functionalized ^{HTL}BSA bNDAs. (H) TIRF microscopy image of HaloTag-mEGFP-IFNAR2 bNDAs in live cell. (I) Intensity profile along the yellow line highlighted in panel H. (J-O) Formation of Lrp6 and Fzd8 nanopatterns in live cells on tdClamp-functionalized ^{HTL}BSA bNDA. (J) Cartoon of capturing mEGFP-Lrp6 by tdClamp and co-recruitment of SNAP-Fzd8 (labeled with ^{Dy647}). (K) Merged TIRF microscopy image of the immobilized mEGFP-Lrp6 (green) on tdClamp functionalized ^{HTL}BSA bNDAs with the co-recruited SNAP-Fzd8 receptor (labeled with ^{Dy647}, blue). (L) Intensity profile along the yellow line highlighted in panel K. (M) Cartoon of capturing mEGFP-Fzd8 to tdClamp bNDAs in presence of co-expressed mScarlet-Lrp6. (N) Merged TIRF microscopy image of mEGFP-Fzd8 NDAs (green) and mScarlet-Lrp6 (blue). (O) Intensity profile along the yellow line highlighted in panel N. Scale bars: 10 µm.

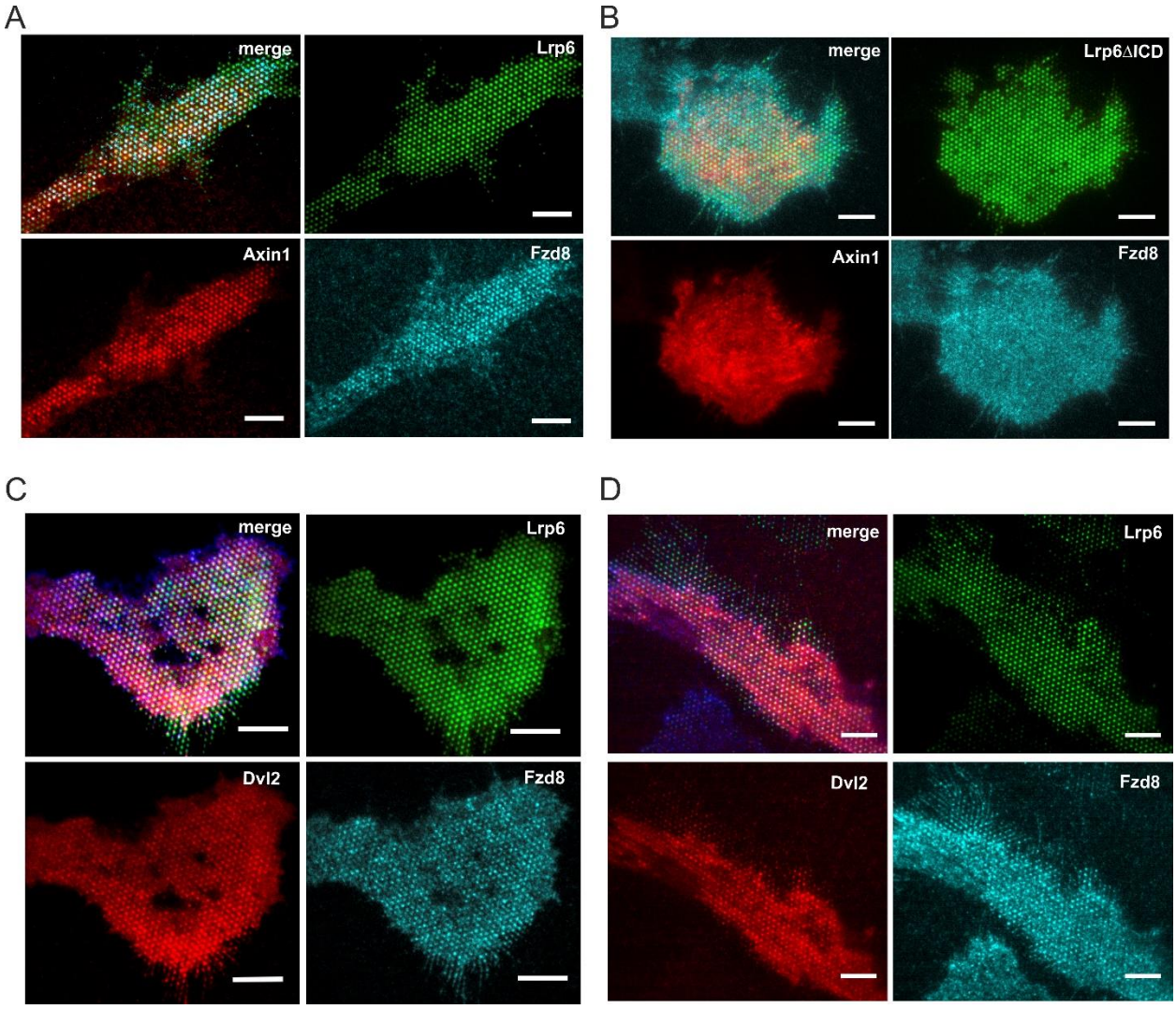

Fig. S3 Whole cell images of co-patterning experiments on tdClamp-functionalized bNDAs. (A) TIRF microscopy image of a wild type (wt) HeLa co-expressing mEGFP-Lrp6 (green), SNAP-Fzd8 labeled with ^{Dy647} (cyan) and tdmCherry-Axin1 (red). (B) TIRF microscopy images of a wild type HeLa cell co-expressing mEGFP-Lrp6ΔICD (green), SNAP-Fzd8 labeled with ^{Dy647} (blue) and tdmCherry-Axin1 (red). (C) TIRF microscopy images of a wild type HeLa cell co-expressing mEGFP-Lrp6 (green), SNAP-Fzd8 labeled with ^{Dy647} (blue) and tdmCherry-Dvl2 (red). (D) TIRF microscopy images of an Axin1/2 double-knock-out HeLa cell co-expressing mEGFP-Lrp6 (green), SNAP-Fzd8 labeled with ^{Dy647} (blue) and Dvl2-tdmCherry (red). Scale bars: 10 µm.

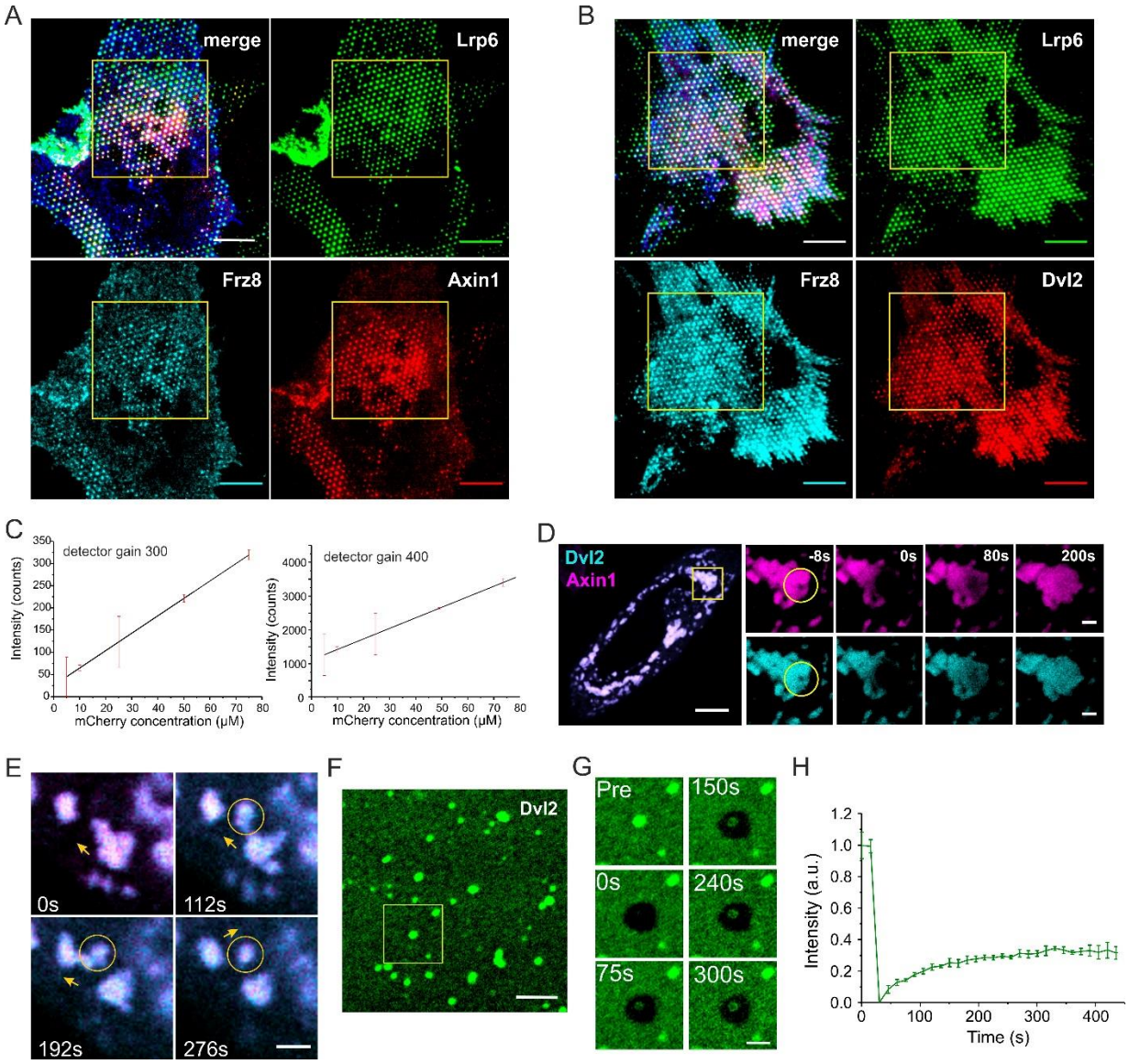

Fig. S4 Dynamics of Axin1 and Dvl2 (co-)condensates. (A, B) Representative full-cell images of Wnt signalodots for FRAP experiments. (A) TIRF images of a wt HeLa cell co-expressing mEGFP-Lrp6 (green), SNAP-Fzd8 labeled with Dy647 (blue) and tdmCherry-mAxin1 (red) prior to FRAP. Scale bars: 10 µm. (B) TIRF images of a HeLa cell co-expressing mEGFP-Lrp6 (green), SNAP-Fzd8 labeled with Dy647 (blue) and Dvl2-tdmCherry (red) prior to FRAP. Scale bars: 10 µm. (C) Calibration plots of intensity-concentration used for quantifying the Dvl2-mCherry concentrations *in cellulo*. Purified mCherry was used in the confocal microscopy measurement with different detector gains. (D) Sub-droplet dynamics of the co-condensation of Axin1 (magenta) and Dvl2 (cyan) characterized by confocal fluorescence microscopy. Scale bar: 2 µm (10 µm in the overview image). (E) Fission and fusion of Axin1/Dvl2 co-condensates captured in time-lapse confocal microscopy (cf. Video S5). (F-H) Dynamics of Dvl2 droplets formed from purified protein in *vitro*. (F) Confocal laser scanning microscopy of 2 µM mEGFP-Dvl2 in HBS buffer. Protein droplets formation was initiated by adding 5% w/w PEG (Mw 3000). Scale bar: 5 µm. (G) Time-lapse microscopy imaging of the photobleached region marked in yellow in panel F. Scale bar 2 µm. (H) FRAP of mEGFP-Dvl2 droplets. Mean±s.d. were obtained from triple experiments.

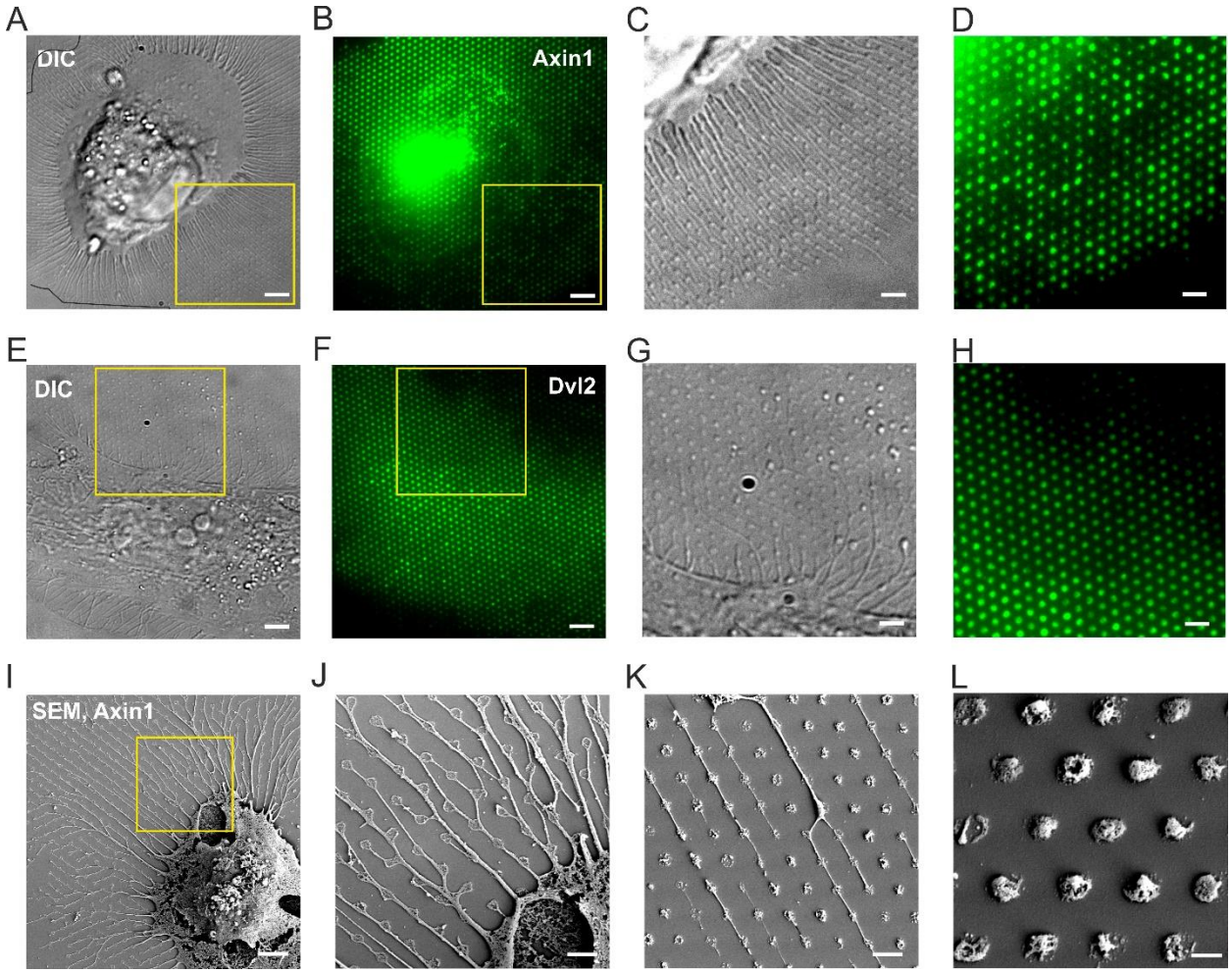

Fig. S5 Intracellular capturing of Axin1 or Dvl2 into bNDAs using artificial transmembrane anchors ALFAnb-TMD-GFPnb. (A-D) Capturing of Axin1 on bNDAs in HeLa cells. (A) Differential interference contrast (DIC) image of a HeLa cell co-expressing mEGFP-Axin1/SNAP-Fzd8 showing distinct mEGFP-Axin1 nanodroplet arrays. (B) TIRF microscopy image of mEGFP-Axin1 in the cell. Scale bars: 5 µm. (C, D) Zoom-up DIC image (C) and TIRF microscopy image (D) of the highlighted area. Scale bars: 2 µm. (E-H) Formation of Dvl2 bNDAs using artificial transmembrane anchors. (E) DIC image of a HeLa cell co-expressing mEGFP-Dvl2/SNAP-Fzd8 showing mEGFP-Dvl2 phase separation in nanodroplets arrays. (F) TIRF microscopy image of mEGFP-Dvl2 in the cell. Scale bars: 5 µm. (G, H) Zoom-up DIC image (G) and TIRF microscopy image (H) of the highlighted area in (E). Scale bars: 2 µm. (I-L) Scanning electron microscopy (SEM) images of a mEGFP-Axin1/SNAP-Fzd8 co-expressing HeLa cell on bNDAs. (I) SEM of a fixed HeLa cell with mEGFP-Axin1 nanodroplet arrays. Scale bar: 3 µm. (J) Zoom-up image of the highlighted area in (I). Scale bar: 1 µm. (K) Another representative SEM image of mEGFP-Axin1 bNDAs. Scale bar: 1 µm. (L) SEM image of individual mEGFP-Axin1 nanodroplets. Scale bar: 500 nm.

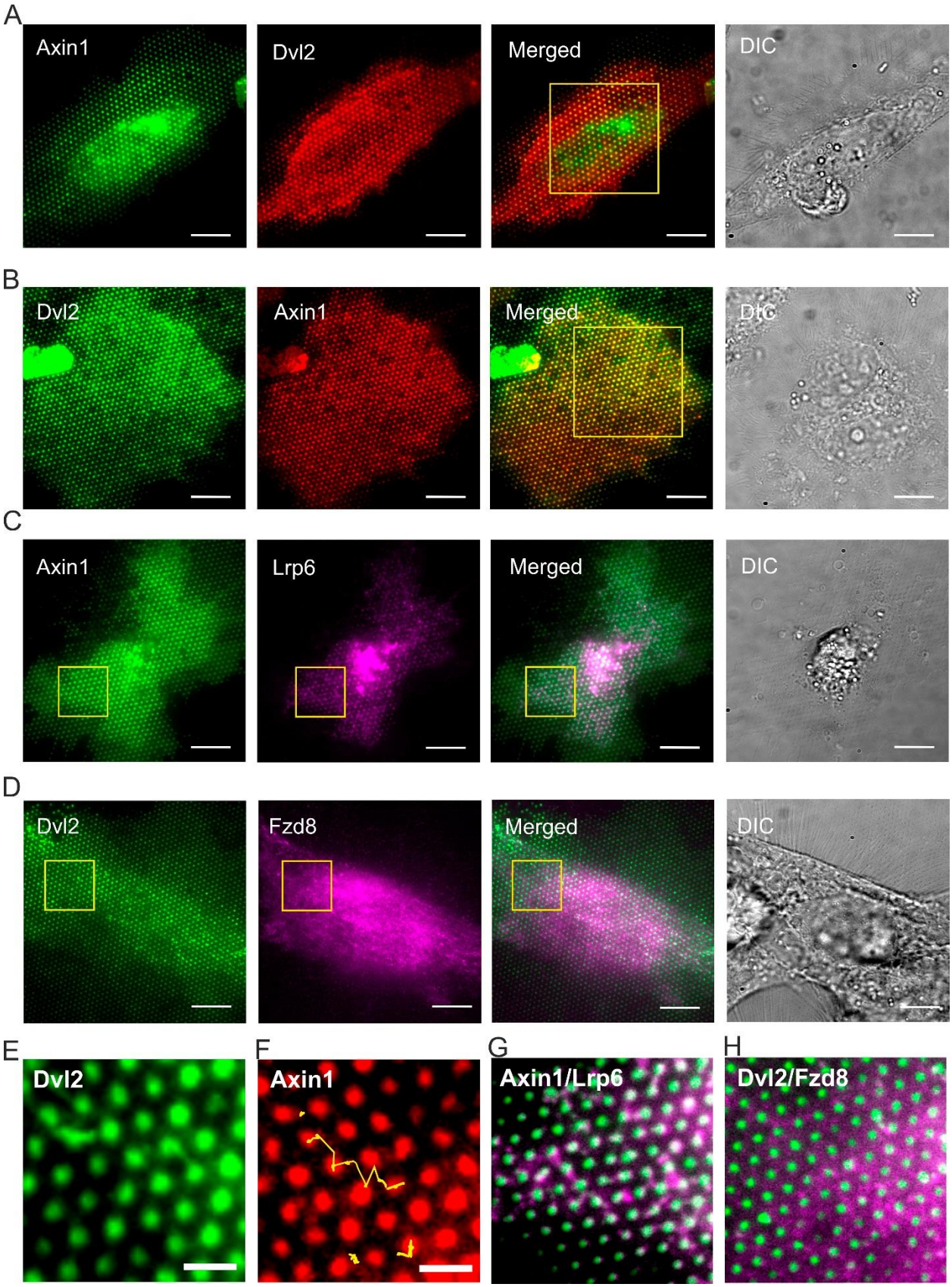
A
Axin1
Dvl2
Merged
DIC
B
Dvl2
Axin1
Merged
DIC
C
Axin1
Lrp6
Merged
DIC
D
Dvl2
Fzd8
Merged
DIC
E
Dvl2
F
Axin1
G
Axin1/Lrp6
H
Dvl2/Fzd8

Fig. S6 Condensations of Axin1 and Dvl2 and their interactions with co-receptors in Axin DKO HeLa cell. (A) Dual-color TIRF microscopy images of mEGFP-Axin1 bNDA (green) and Dvl2-tdmCherry (red). (B) Dual-color TIRF microscopy images of mEGFP-Dvl2 bNDA (green) and tdmCherry-Axin1 (red). Scale bars: 10 µm. Yellow box marks the FRAP region. (C) Dual-color TIRF microscopy images of mEGFP-Axin1 bNDA (green) and mScarlet-Lrp6 (magenta). (D) Dual-color TIRF microscopy images of mEGFP-Axin1 bNDA (green) and mScarlet-Fzd8 (magenta). Scale bars: 10 µm. Yellow boxes mark region for correlation analysis. (E, F) Intensity projection of 240 time-lapse TIRF microscopy images for Dvl2 and Axin1 nanodroplets. Image acquisition rate: 1fps. (E) Dvl2-mEGFP nanodroplets (green). (F) tdmCherry-Axin1 nanodroplets (red). Scale bars: 2µm. Droplet dynamic of Axin1 between bNDAs was marked by yellow trajectories. (G, H) Zoom-up of the highlighted regions in the merge images of (C) and (D). Scale bars: 2 µm.

SUPPLEMENTARY VIDEOS

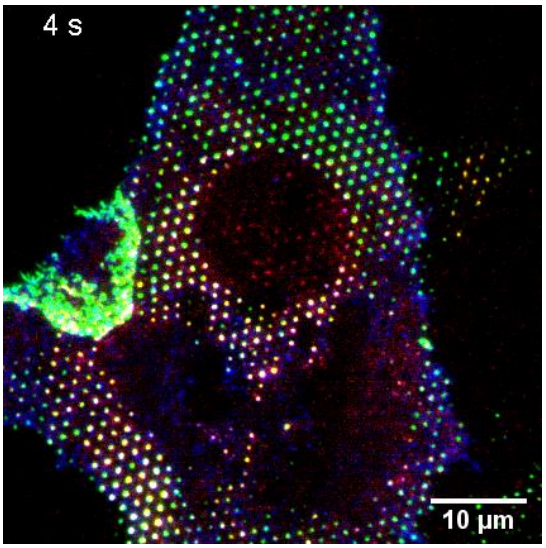

Video S1 TIRF microscopy of fluorescence recovery after photobleaching of tdmCherry-Axin1(red) on mEGFP-Lrp6 (green)/SNAP-Fzd8(blue) nanodot array. Scale bar: 10 µm.

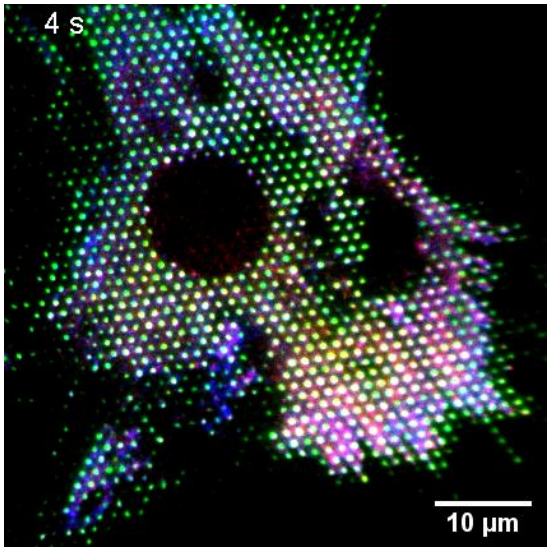

Video S2 Time-lapse TIRF microscopy of FRAP for quantifying the dynamics of Dvl2-tdmCherry (red) on mEGFP-Lrp6 (green)/SNAP-Fzd8(blue) nanodot array. Scale bar: 10 µm.

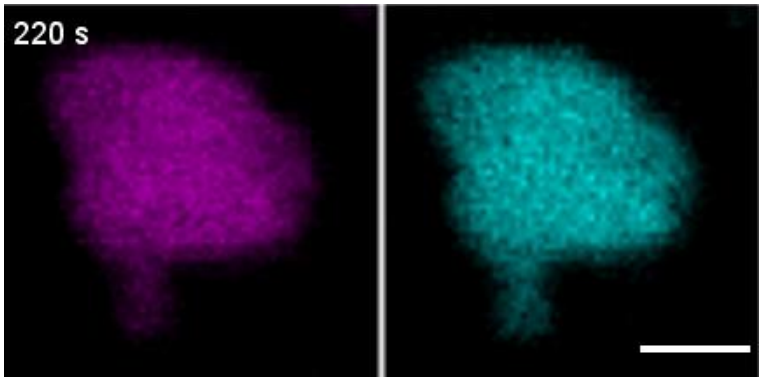

Video S3 FRAP experiment of a ^{SiR}HaloTag-Axin1 (magenta)/Dvl2-tdmCherry (cyan) co-condensate in the cytosol of a HeLa cell. Scale bar: 2 µm.

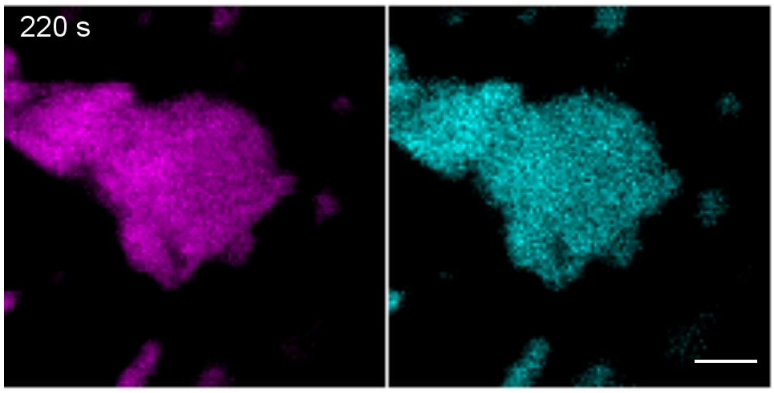

Video S4 Time-lapse confocal microscopy imaging of sub-droplet FRAP in ^{SiR}HaloTag-Axin1 (magenta)/Dvl2-tdmCherry (cyan) co-condensates in a HeLa cell. Scale bar: 2 µm.

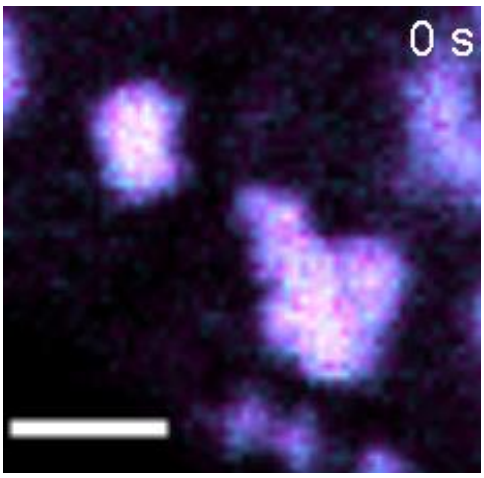

Video S5 Time-lapse confocal microscopy imaging of the dividing and coalescing of ^{SiR}HaloTag-Axin1 (magenta)/Dvl2-tdmCherry (cyan) co-condensates in a HeLa cell. Scale bar: 2 µm.

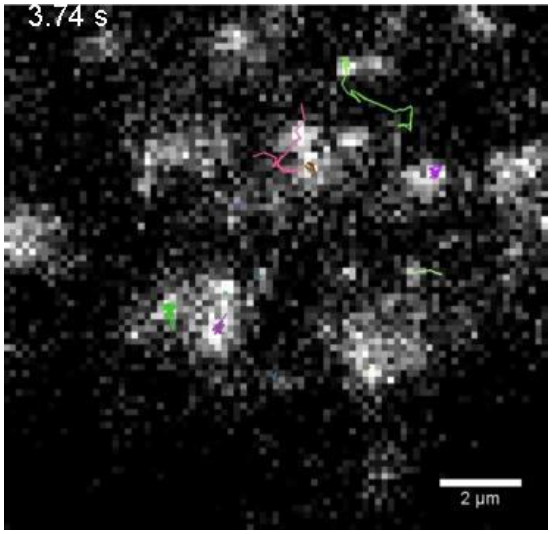

Video S6 Single molecule tracking of individual Dvl2-HaloTag molecules in Dvl2-^{SiR}HaloTag/Dvl2-tdmCherry droplet in a HeLa cell. Scale bar: 2 µm.

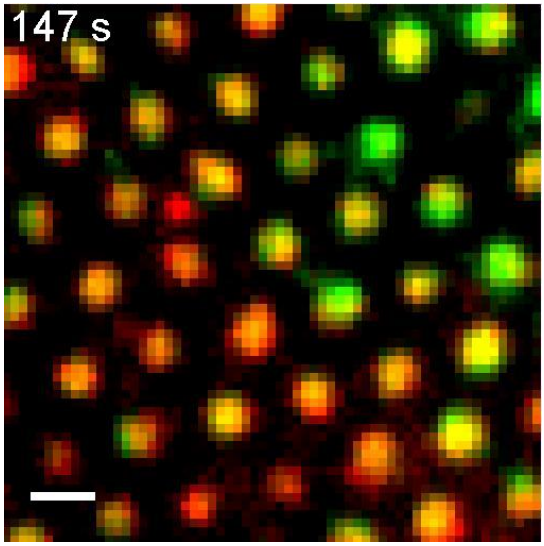

Video S7 Time-lapse TIRF imaging of tdmCherry-Axin1 nanodroplet arrays (red) generated by direct capturing of Dvl2-mEGFP (green) into bNDAs of an Axin1/2 DKO HeLa cell. Scale bar: 1 µm.

SUPPLEMENTARY TABLE

Table S1 Summary of association rate constants k_{on} determined by TIRFS-RIF detection.

Protein	**Surface**	**k_{on} ($M^{-1}s^{-1}$)***
BSA	DMDCS	$(1.05\pm0.18)\times10^4$
	OTS	$(9.75\pm0.01)\times10^3$
	DPDCS	$(1.44\pm0.03)\times10^4$
	NMTS	$(2.73\pm0.28)\times10^5$
HaloTag	^{HTL}BSA	$(3.26\pm0.01)\times10^3$
mEGFP	tdClamp	$(8.14\pm0.08)\times10^4$
ALFAnb	^{ALFA}BSA	$(2.02\pm0.05)\times10^4$

* Data presented as mean ± S.E. of curve fittings.

Table S2 Description of the plasmids used for live cell bNDA experiments.

Plasmid name	**Protein name**	**Insert (from N to C)**
pSems-HaloTag-mEGFP-IFNAR2	HaloTag-mEGFP-IFNAR2	IgκLS[a]-HaloTag[b]-mEGFP[c]-IFNAR2
pSems-leader-mEGFP-hLrp6	mEGFP-Lrp6	IgκLS- mEGFP-hLrp6
pSems-leader-mEGFP-hLrp6ΔICD	mEGFP-Lrp6ΔICD	IgκLS-mEGFP[c]-hLrp6ΔICD
pSems-puro-leader-mScarlet-hLrp6	mScarlet-Lrp6	IgκLS-mScarlet-hLrp6
pSems-leader-fSNAP-mFzd8	SNAP-Fzd8	IgκLS- fSNAP[d]-mFzd8
pSems-leader-mEGFP-mFzd8	mEGFP-Fzd8	IgκLS- mEGFP-mFzd8
pSems-leader-mScarlet-mFzd8	mScarlet-Fzd8	IgκLS- mScarlet-mFzd8
pSems-tdmCherry-linker-mAxin1	tdmCherry-Axin1	tdmCherry-linker-mAxin1
pSems-mTagBFP-GSlinker-mAxin1	mTagBFP-Axin1	mTagBFP-GSlinker-mAxin1

pSems-mEGFP-GSlinker-mAxin1	mEGFP-Axin1	mEGFP-GSlinker-mAxin1
pSems-HaloTag-GSlinker-mAxin1	HaloTag-Axin1	HaloTag-GSlinker-mAxin1
pSems-puro-Dvl2-tdmCherry / mCherry	Dvl2-tdmCherry / mCherry	Dvl2-tdmCherry / mCherry
pSems-Dvl2-linker-mEGFP	Dvl2-mEGFP	Dvl2-linker-mEGFP
pSems-leader-aALFAnb-TMD-antiGFPnb	aALFA-TMD-aGFPnb	IgκLS-antiALFAnanobody-Transmembrane domain[e]-antiGFPnanobody

[a] IgκLS: leader sequence of the murine Igκ chain taken from the pDisplay vector (Invitrogen).
[b]HaloTag: The HaloTag7 gene was amplified from the vector pFC17A-HaloTag7 (Promega).
[c]mEGFP: monomeric EGFP obtained by the A206K mutation within the EGFP sequence of pEGFP-N1 (Takara Bio Inc.).
[d]SNAP-tag: engineered O^6-alkylguanine-DNA alkyltransferase (Gautier et al., 2008), New England Biolabs, Inc.
[e]Transmembrane domain: Artificial TMD with the sequence of $(ALA)_7$ repeats.

Table S3: List of key materials and suppliers.

Reagent and abbreviation	Source	Catalogue number
1-Napthylmethyl)trichlorosilane (NMTS)	Gelest	SIN6596.0
Diphenyldichlorosilane (DPDCS)	Gelest	SID4510.1
Dichlorodimethylsilane (DMDCS)	Merck	8034520250
Trichloroctadecylsilan (OTS)	Sigma Aldrich	104817
Toluene	Fisher Scientific	14214914
1-Ethyl-3-(3-dimethylaminopropyl)carbodiimide-hydrochloride (EDC)	Carl Roth	2156.2
N-Succinimidyl 13-Maleimido-11-oxo-4,7-dioxa-10-azatridecanoate (Mal-PEG_2-NHS)	Tokyo Chemical Industry	M3079
Albumin Fraction V from bovine serum (BSA)	Carl Roth	0163.1
HTL-NH_2	Own synthesis	Liße, *et al*., 2011
ALFA-peptide (Ac-CPSRLEEELRRRLTE-COOH)	Romer Labs	Custom synthesis
1,4-Dithiothreitol (DTT)	Carl Roth	6908.2
N-2-Hydroxyethylpiperazine-*N*'-2-ethane sulphonic acid (HEPES)	Carl Roth	6763.3
Ethylenediamine tetra-acetic acid (EDTA)	Carl Roth	8040.2

Dulbecco's Modified Eagle's Medium (MEM)	PAN-Biotech	P04-09500
Dulbecco's phosphate buffered saline (PBS)	PAN-Biotech	P04-36500
Fetal bovine serum (FBS)	PAN-Biotech	P30-3031
NaCl	Carl Roth	3957.1
Imidazole	Carl Roth	3899.4
Isopropyl-β-D-thiogalactopyranoside (IPTG)	Thermo Fisher Scientific	R0392
DNase	Sigma Aldrich	DN25
Lysozyme	Sigma Aldrich	L6876
Urea	Carl Roth	3941.2
Protease inhibitor	Serva	39106
Chloramphenicol	Biomol	C4350.25
Ampicilin	Biomol	01503.25
Trypsin	Capricorn Scientific	TRY-1B
ViaFect™	Promega	E4982
Linear polyethylenimine hydrochloride (PEI)	Polysciences	24765-1
2-Amino-2-(hydroxymethyl)propane-1,3-diol (TRIS)	Sigma Aldrich	8.01464
Catalase	Sigma Aldrich	C-40
Glucose	Carl Roth	3774.1
Glucose oxidase	Sigma Aldrich	49180
Glutaraldehyde	Electron Microscopy Sciences	16216
β-Mercaptoethanol	Sigma Aldrich	63689
6-bromoindirubin-3-oxime (BIO)	Sigma Aldrich	B1686
Monoclonal β-Catenin Mouse Antibody – Alexa Flour 647 Conjugate	Cell Signaling Technology	4627S
Silicon Rhodamine HaloTag-Ligand (SiR-HTL)	Kai Johnsson's Lab	Lukinavičius G., *et al*., 2013
ATTO647N-NHS ester	ATTO-TEC GmbH	AD 647N-31
SNAP-Surface®549	New England Biolabs	S9112S
SNAP-Surface®647	New England Biolabs	Discontinued and replaced by SNAP-Surface® 649, S9159S